Valence-shell single photoionization of Kr^+ ions: Experiment and theory

G. Hinojosa,* A. M. Covington, G. A. Alna'Washi,† M. Lu, and R. A. Phaneuf
Department of Physics, University of Nevada, Reno, Nevada 89557-0220, USA

M. M. Sant'Anna
Instituto de Física, Universidade Federal do Rio de Janeiro, Caixa Postal 68528 – CEP, 21941-972 Rio de Janeiro RJ, Brazil

C. Cisneros and I. Álvarez
Instituto de Ciencias Físicas, Universidad Nacional Autónoma de México, Apartado Postal 48-3, Cuernavaca 62210, Morelos, México

A. Aguilar, A. L. D. Kilcoyne, and A. S. Schlachter
Advanced Light Source, Lawrence Berkeley National Laboratory, 1 Cyclotron Road, Berkeley, California 94720, USA

C. P. Ballance
Department of Physics, 206 Allison Laboratory, Auburn University, Auburn, Alabama 36849-5311, USA

B. M. McLaughlin‡
Institute for Theoretical Atomic and Molecular Physics, Harvard Smithsonian Center for Astrophysics, 60 Garden Street, MS-14, Cambridge, Massachusetts 02138, USA

(Received 11 September 2012; published 5 December 2012)

Photoionization of Kr^+ ions was studied in the energy range from 23.3 to 39.0 eV at a photon energy resolution of 7.5 meV. Absolute measurements were performed by merging beams of Kr^+ ions and of monochromatized synchrotron undulator radiation. Photoionization (PI) of this Br-like ion is characterized by multiple Rydberg series of autoionizing resonances superimposed on a direct PI continuum. Resonance features observed in the experimental spectra are spectroscopically assigned and their energies and quantum defects tabulated. The high-resolution cross-section measurements are benchmarked against state-of-the-art theoretical cross-section calculations from the Dirac-Coulomb *R*-matrix method [J. Phys. B **45**, 085701 (2012)].

DOI: 10.1103/PhysRevA.86.063402 PACS number(s): 32.80.Fb, 32.80.Zb, 32.80.Ee

I. INTRODUCTION

The identification of spectroscopic lines from ions is crucial for studying practically all regions of the universe, as most of the matter in the interstellar medium is in an ionized state [1]. The photoionization of krypton ions is of particular interest in the determination of elemental abundances in stars and planetary nebulae [2], as well as in inertial-confinement fusion experiments [3]. Injection of Kr gas has been demonstrated to mitigate disruption in magnetically confined Tokamak fusion plasmas [4].

Spectroscopic lines of Kr ions have been used as markers in nebular spectroscopy, a developing field that promises to help understand evolutionary models of stars [5]. In planetary nebulae, the known emission line of Kr III (Kr^{2+}): $4s^24p^4(^3P_2) \rightarrow 4s^24p^4(^1D_2)$ has been used to identify Kr which is a characteristic element resulting from the process of nucleosynthesis in stars [2,6,7], where up to 6 times ionized Kr ion stages have been detected.

For some of these ions, photoionization (PI) parameters have been measured; Kr^+ [3], Kr^{3+} [8], Kr^{5+} [9], the Kr isoelectronic sequence [10], *K*-shell photoionization of Kr^+ [11], and extreme UV radiation photoionization [12,13].

A significant increase of the available photon flux from third-generation synchrotron light sources has allowed an important technical limitation due to the tenuousness of ion beam targets to be surmounted for a number of atomic ions [14,15]. This development has made accurate experimental data on ionic structure available to benchmark state-of-the-art quantum mechanical models.

Sophisticated methods are available for the calculation of PI cross sections [16–18]; high-resolution measurements are required to verify theoretical predictions [19] or reveal the limitations of a particular model. High-resolution Xe^+ PI data were successfully used to benchmark the Dirac atomic *R*-matrix codes (DARC) [20]. The availability of better atomic structure for these ion stages [14,15] has prompted the refinement and development of better photoionization models [5,20]. Although the agreement between theory and experiment has improved, the accurate description of the PI process is still far from trivial because it requires a detailed analysis of all open and closed interfering channels.

Relevant to this work are the pioneering PI studies of isoelectronic atomic Bromine carried out by Ruščić *et al.* [21] and

*Present address: Instituto de Ciencias Físicas, Universidad NacionalAutónoma de México, Apartado Postal 48-3, Cuernavaca 62210, Morelos, México; hinojosa@fis.unam.mx

†Present address: Department of Physics, The Hashemite University, Zarqa 13115, Jordan; alnawashi@hu.edu.jo

‡Present address: Centre for Theoretical Atomic, Molecular and Optical Physics (CTAMOP), School of Mathematics and Physics, The David Bates Building, 7 College Park, Queen's University of Belfast, Belfast BT7 1NN, United Kingdom; b.mclaughlin@qub.ac.uk

by van der Meulen *et al.* [22]. Both these measurements were conducted at lower photon energy resolution than in the present experiment but permitted measurement and identification of autoionizing Rydberg series converging to final states of Br^+, $4s^24p^4(^3P_{0,1,2}, {}^1D_2\ {}^1S_0)$, and $4s4p^5(^3P^o_{0,1,2})$, which guided the spectroscopic assignments in the present photoionization measurements of Kr^+ ions.

Similar measurements of photoionization of Kr^+ were carried out by Bizau *et al.* [3] at a photon energy resolution ranging between 50 meV near the ground-state ionization threshold of 24.36 eV, and 100 meV at photon energies 15 eV above threshold. They were also able to perform measurements in the photon energy range 23.0–27.0 eV with a spectral resolution of 30 meV. Although their merged-beam measurements were normalized to ground-state cross sections from ion trap measurements, the resonance structure could not be fully resolved and spectroscopically assigned. With that objective, the present measurements were taken with spectral resolution of 7.5 meV in the energy range 23.3–39.0 eV.

The ASTRID measurements for absolute cross sections permitted comparison with theoretical calculations performed using the MCDF method. Bizau and co-workers identified Rydberg resonance series $4s^24p^4(^1D_2, {}^1S_0)nd$ that converged to the $^1D_2$ and $^1S_0$ thresholds. PI cross-section calculations using the DARC on this system have recently been performed by McLaughlin and Ballance [20] in the near-threshold region, which showed excellent agreement with the absolute PI measurements made at the ASTRID and SOLEIL synchrotron radiation facilities. In the present higher resolution work, it was possible to resolve, identify, and reassign a wealth of resonance structure. Theoretical results on this complex help interpret, benchmark, and validate experimental measurements.

II. EXPERIMENT

The experiment was conducted on undulator beamline 10.0.1.2 of the Advanced Light Source (ALS) at Lawrence Berkeley National Laboratory, using the ion-photon-beam (IPB) end station based on the merged-beams technique [23]. The experimental method has been described in detail elsewhere in previous measurements of photoionization cross sections for Ne^+ [24], CO^+ [25], and O^+ [26,27].

A. Photon beam

A grazing-incidence spherical-grating monochromator dispersed the light generated by a 10-cm period undulator, delivering a highly collimated photon beam of spatial width less than 1 mm and divergence less than 0.5°. The beamline delivers a maximum flux of 5×10^{12} photons per second in a bandwidth of 0.01% at an energy of 30 eV. In the energy range of 23.3–34.0 eV a spectral resolution of 7.5 meV was selected by adjusting the entrance and exit slits of the monochromator. Figure 1 shows an overview of the spectra obtained at the resolution of 7.5 meV over the photon energy range 23.0–39.0 eV.

The photon energy was scanned by rotating the grating and translating the exit slit of the monochromator, while simultaneously adjusting the undulator gap to maximize the beam intensity. The photon flux was measured by an absolutely calibrated silicon x-ray photodiode. The analog output from a precision current meter was directed to a voltage-to-frequency converter, which provided a normalization signal to a personal-computer-based data acquisition system. The photon beam was time modulated (mechanically chopped) at 0.5 Hz using a stepping-motor controlled paddle to separate photoions from background produced by stripping of the parent Kr^+ ion beam on residual gas in the ultrahigh vacuum system. The photon energy scale was calibrated using measurements of the known O^+ ground-state ($^4S^o$) and metastable-state ($^2P^o$ and $^2D^o$) energy thresholds [26,27], allowing for the Doppler shift due to the ion motion in the laboratory frame of reference. The absolute uncertainty in the photon energy scale is estimated to be ±30 meV.

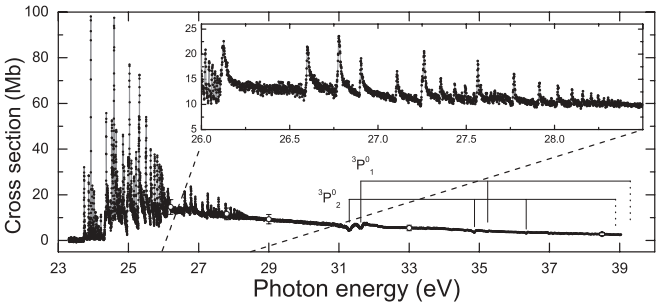

FIG. 1. An overview of single photoionization cross-section measurements from the ALS of Kr^+ ions as a function of the photon energy. The data were taken with a nominal energy resolution of 7.5 meV. Two assigned Rydberg series are indicated as vertical lines grouped by horizontal lines. The corresponding series limits E_∞ of Eq. (4) for each series are indicated by vertical-dashed lines in the end of the line groups. Labels correspond to two final states generated from initial ground state $Kr^+(^2P^o_{3/2})$. Identified resonance features of this graphic are tabulated in Table II. The inset shows the low-energy region on an expanded energy scale. Assignments at lower energies are shown in Fig. 3 which is a smaller range of the same spectrum. The ALS absolute measurements given in Table I are shown as open circles.

B. Ion beam

Kr^+ ions were produced in a hot-filament discharge ion source. The filament was mounted inside a small chamber filled with Kr gas to a constant pressure of typically 0.1 Torr. A metallic cap (anode) with a 1-mm diameter hole (exit) placed as a cover, allowed ions to be extracted from the chamber and isolated the higher pressure region of the ion source from the high vacuum in the extraction region. Electrons emitted by the filament were accelerated by a potential difference of 100 V applied between the filament and the anode. Electron-atom collisions at energies $\leqslant$100 eV are the main mechanism for production of Kr^+ ions.

Kr^+ ions extracted from the ion source were accelerated to an energy of 6.0 keV, forming a beam that was electrostatically focused and mass-to-charge selected by a 60° sector magnet.

The surrounding volume inside the exit of the ion source chamber is a region of undetermined high pressure where ions suffered low energy resonant collisions with neutral Kr and residual gas molecules. It is well known that in certain

collision systems, the relative populations of the $^2P^o_{3/2}$ and $^2P^o_{1/2}$ metastable states of noble gas ions may be controlled by collisional quenching at thermal energies [28].

To our knowledge, collisional quenching of metastable $Kr^+(^2P^o_{1/2})$ has only been tested for collisions with CH_4 [29]. No clear experimental evidence was found that such collisions actually modify the relative populations of the ground and metastable states. However, the strong evidence of metastable collisional quenching of the $Xe^+(^2P^o_{1/2})$ metastable state in collisions with N_2O and CH_4 supports the possibility that resonant collisions of Kr^+ with Kr atoms or vacuum remanent residual gas molecules may reduce the population of the initial $Kr^+(^2P^o_{1/2})$ metastable state.

C. Beam-beam interaction

Two cylindrical einzel lenses and a set of four-jaw slits focused and collimated the Kr^+ ion beam. With the aid of two sets of perpendicular electrostatic steering plates, the ion beam was positioned and directed toward a 90° electrostatic spherical-sector deflector that merged the well-collimated ion beam onto the axis of the counterpropagating photon beam from the ALS. Typical diameter of the photon beam was 0.1 cm; the ion beam diameter varied between 0.2 and 0.5 cm.

The interaction region consisted of an electrically isolated stainless-steel-mesh cylinder to which an electric potential of +2 kV was applied to energy-label Kr^{2+} ions produced within. Entrance and exit apertures accurately defined the effective length of the interaction region (29.4 ± 0.6 cm). Two-dimensional intensity distributions of both beams were measured by commercial rotating-wire beam profile monitors installed along the merged path just upstream and downstream of the interaction region, and by a translating-slit scanner located at the center of the region. The profile monitors permitted the positions and spatial intensity profiles of the two beams to be continuously monitored on an oscilloscope while tuning the beams for optimum overlap. The pressure in this region was typically 5×10^{-10} Torr under measurement conditions.

D. Separation and detection of product ions

Downstream of the interaction region, a 45° dipole analyzing magnet demerged the beams and separated the Kr^{2+} products from the parent Kr^+ beam, which was collected in an extended Faraday cup. The magnetic field was set such that the Kr^{2+} product ions passed through an aperture in the back of the Faraday cup. A spherical 90° electrostatic deflector directed them onto a stainless steel plate biased at −550 V, from which secondary electrons were accelerated and detected by a microsphere-plate electron multiplier operated in pulse-counting mode.

The detection planes of the demerger magnet and this spherical detector are orthogonal, permitting the Kr^{2+} products to be swept across the detector in mutually perpendicular directions, providing a diagnostic of their complete collection. The absolute efficiency of the photoion detector was calibrated *in situ* using an averaging subfemtoampere meter to record the Kr^{2+} photoion current, which was then compared to the measured photoion count rate. The primary Kr^+ ion beam current was measured by a precision current meter, whose analog output was directed to a voltage-to-frequency converter, providing a normalization signal to the data acquisition system.

III. THEORY

For comparison with high-resolution measurements made at the ALS, state-of-the-art theoretical methods using highly correlated wave functions are required that include relativistic effects as fine-structure effects may be resolved. An efficient parallel version [30] of the DARC [31–34] suite of codes has been developed [20,35,36] to address the challenge of electron and photon interactions with atomic systems catering for hundreds of levels and thousands of scattering channels. Metastable states are populated in the Kr^+ ion beam and require additional theoretical calculations to be carried out. Modifications to the Dirac atomic *R*-matrix codes [20,35,36] allowed high quality photoionization cross-section calculations to be made on heavy complex systems of prime interest to astrophysics and plasma applications. Cross-section calculations for *trans*-Fe element single photoionization of Se^+ and Xe^+ ions along with low ionization stages of W ions [20,36,37] have been made.

Photoionization cross sections on this halogen-like ion were performed for the ground and the excited metastable levels associated with the $4s^24p^5$ configuration for Kr^+ to benchmark the theoretical results and validate the present high-resolution experimental measurements made at the Advanced Light Source radiation facility in Berkeley. Details of the atomic structure calculations with the GRASP code can be found in our recent work on this complex ion [20] where a detailed comparison was made for the PI cross sections with the measurements performed at the ASTRID and SOLEIL radiation facilities. In the photoionization cross-section calculations for this complex *trans*-Fe element all 326 levels arising from the seven configurations, $4s^24p^4$, $4s4p^5$, $4s^24p^34d$, $4s^24p^24d^2$, $4p^6$, $4s4p^44d$, and $4p^44d^2$, were included in the close-coupling expansion. PI cross-section calculations with this 326-level model were performed in the Dirac-Coulomb approximation using the DARC codes [20,36].

The *R*-matrix boundary radius of 7.44 Bohr radii was sufficient to envelop the radial extent of all the $n = 4$ atomic orbitals of the residual Kr^{2+} ion. A basis of 16 continuum orbitals was sufficient to span the incident experimental photon energy range from threshold up to 40 eV. Since dipole selection rules apply, total ground-state photoionization requires only the bound-free dipole matrices, $J^\pi = 3/2^\circ \rightarrow J^{\pi'} = 1/2^e, 3/2^e, 5/2^e$. For the excited metastable states only the $J^\pi = 1/2^\circ \rightarrow J^{\pi'} = 1/2^e, 3/2^e$ are necessary.

For both the ground and metastable initial states, the outer region electron-ion collision problem was solved (in the resonance region below and between all thresholds) using a suitably chosen fine energy mesh of 5×10^{-8} Rydbergs (≈0.68 μeV) to fully resolve all the extremely narrow resonance structure in the appropriate photoionization cross sections. The *jj*-coupled Hamiltonian diagonal matrices were adjusted so that the theoretical term energies matched the recommended experimental values of NIST [38]. We note that this energy adjustment ensures better positioning of certain

resonances relative to all thresholds included in the calculation [20]. Further details of the theoretical calculations can be found in our recent work on this complex ion [20], using the modified DARC codes, that showed suitable agreement with the experimental data of Bizau and coworkers [3].

In the present work the DARC PI cross-section calculations were convoluted with a Gaussian of 7.5 meV FWHM and statistically weighted for the ground and metastable states to compare directly with the higher-resolution PI measurements performed at the Advanced Light Source synchrotron radiation facility in Berkeley.

IV. RESULTS

A. Cross-section measurements

Absolute photoionization measurements were carried out at a number of discrete photon energies where resonant structure was absent. The values of the effective photoionization cross section $\sigma_{\rm PI}$ [cm^2] were determined from experimental parameters:

$$\sigma_{\rm PI} = \frac{Rqe^2 v_i \epsilon}{I^+ I^\gamma \Omega \tau \Delta \int F(z)dz}, \qquad (1)$$

where R is the photoion count rate [s^{-1}], q is the charge state of the parent ion, $e = 1.60 \times 10^{-19}$ C, v_i is the ion beam velocity [cm s^{-1}], ϵ is the responsivity of the photodiode [electrons/photon], I^+ is the parent ion beam current [A], I^γ is the photodiode current [A], Ω is the photoion collection efficiency, τ is the pulse transmission fraction of the photoion detection electronics (determined by the pulse discriminator setting), and Δ is the measured absolute photoion detection efficiency. The propagation direction of the ion beam is defined as the z axis. The beam overlap integral $F(z)dz$ denotes the spatial overlap of the photon and ion beams along their common interaction path in units of cm^{-1}. At each of the three positions z_i at which beam intensity profiles were measured, the form factor $F(z_i)$ was determined by the following relation,

$$F(z_i) = \frac{\iint I^+(x,y) I^\gamma(x,y) dxdy}{\iint I^+(x,y)dxdy \iint I^\gamma(x,y)dxdy}. \qquad (2)$$

The present results (see Table I for absolute values) together with measurements made at ASTRID [3] are shown in Fig. 2. Both measurements correspond to an undetermined

TABLE I. Measured values of the total absolute cross section for photoionization of Kr^+ ions from the Advanced Light Source synchrotron radiation facility in Berkeley. The total systematic uncertainties are estimated at a level consistent with 90% confidence level on statistical uncertainties [18,24]. These absolute values are plotted as open circles in Figs. 1, 2, 4, and 5. Note that 1 Mb = 10^{-18}cm^2.

Energy (eV)	Cross section (Mb)
26.2	14.6 ± 4.4
27.8	11.7 ± 3.5
29.0	9.3 ± 2.8
33.0	5.5 ± 1.7
38.5	2.8 ± 0.8

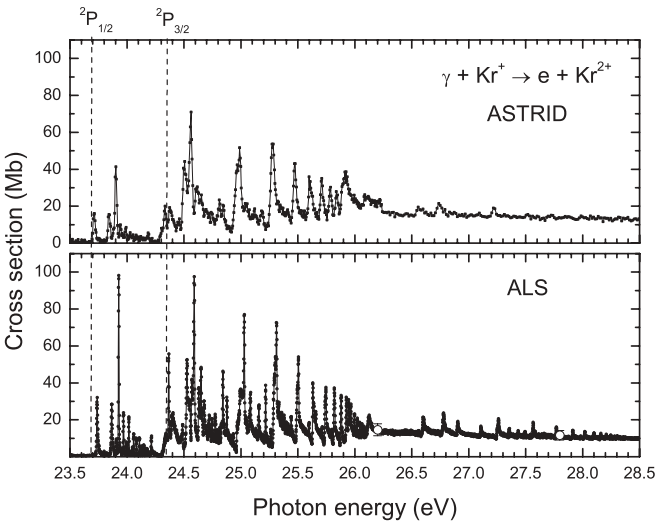

FIG. 2. Comparison of present absolute cross-section measurements for single photoionization of Kr^+ taken at 7.5-meV resolution at ALS with absolute measurements of Bizau *et al.* [3] measured at ASTRID with a resolution of 30 meV. The ALS absolute measurements are shown as open circles.

population-weighted sum of the cross sections for photoionization from the $^2P^o_{3/2}$ ground state and from the $^2P^o_{1/2}$ metastable state of Kr^+. Multiconfiguration Dirac-Fock (MCDF) cross-sections calculations were shown to compare favorably with the ASTRID measurements, for direct (nonresonant) photoionization [3], assuming a statistically weighted population of levels of the $4s^2 4p^5$ configuration in the Kr^+ ion beam. In the present investigation we compare the higher resolution ALS measurements with state-of-the-art cross-section calculations performed using a Dirac R-matrix Coulomb approximation [20] and with the earlier measurements made at ASTRID [3].

The present absolute cross-section measurements are systematically lower than those of Bizau *et al.* [3]. The differences range from about 15% at 26.2 eV to a maximum difference of about 30% at 38.5 eV which is at the upper limit of their combined absolute uncertainties. Even at photon energies high above the ground-state threshold, the measured nonresonant cross section is expected to be relatively insensitive to the admixture of ground and metastable states. Differences between the measured absolute cross sections are attributed to a possible overestimate of the absolute photon flux in the present experiment, caused by an undetermined small fraction of higher-order radiation from the undulator that was dispersed by the monochromator and recorded by the photodiode with higher sensitivity.

Figure 2 presents a comparison of the ALS and ASTRID cross-section measurements in a photon energy range extending about 5 eV above the ionization threshold, emphasizing the effect of photon energy resolution.

A source of uncertainty when interpreting the measurements is the presence of an undetermined mixture of the $^2P^o_{1/2}$ metastable and the $^2P^o_{3/2}$ ground states in the population of the initial Kr^+ ion beam. By combining merged beams and ion-trap techniques, Bizau *et al.* succeeded in extracting pure ground-state absolute cross-section values. Because the ion source used for the present measurements is expected to cause

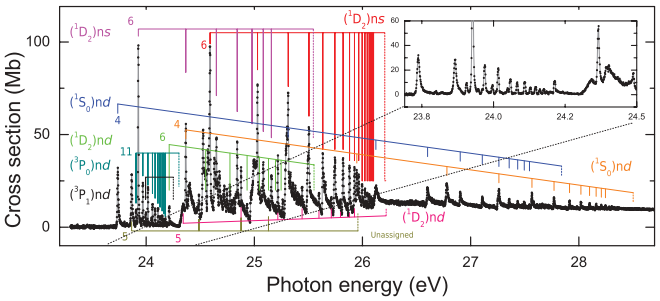

FIG. 3. (Color online) Single photoionization measurements from the ALS of Kr^+ ions as a function of the photon energy measured with a nominal energy resolution of 7.5 meV. The assigned Rydberg series are indicated as vertical lines grouped by horizontal or inclined lines. The corresponding series limits E_∞ of Eq. (4) for each series are indicated by a vertical-dashed line in the end of the line groups. Labels to the left correspond to final states of series generated from initial metastable $Kr^+(^2P^o_{1/2})$. Labels to the right correspond to final states of series generated from ground state $Kr^+(^2P^o_{3/2})$. The first value of n for each series is displayed close to its corresponding vertical line in each group. Gaussian fit centers to the peaks are tabulated in Tables III–V. The inset shows the low-energy region on an expanded energy scale.

some quenching of metastable states, the ground-state fraction may exceed the value of 2/3 based on the relative statistical weights of these two levels. The small differences between the two independent measurements are attributed mainly to systematic uncertainties in both experiments. The sources of uncertainty in the present experiment are comparable in relative magnitudes to those quoted in Refs. [24] and [18]. We also estimate an absolute energy calibration uncertainty of 30 meV in the ALS spectra for this ion.

B. Resonance structure

All the PI cross-section results determined at the ALS with a 7.5-meV spectral resolution (in the photon energy range of 23.3–39.0 eV) are plotted in Fig. 1. In order to help guide the eye, a shorter range of the same spectrum is shown in Fig. 3.

Identification of resonance structures converging to the higher energy limits measured here are shown in Fig. 1 and in Table II. These Rydberg resonance series converge to the $Kr^{2+}(4s4p^5)$ $^3P^o_2$, $^3P^o_1$ series limit and appear as window resonances that are well resolved for $n = 3$ and 4. They are not well resolved for higher quantum number n and the energy difference between both states is 0.412 ± 0.030 eV, which is to be compared with the value of 0.428 eV tabulated by NIST.

In Fig. 3 a wealth of resonance structure is shown together with the proposed assignments to the most prominent features in the spectrum. In Tables II–V values of Gaussian fit centers to the peaks are listed according to their assignments. The identified resonances are consistent with Rydberg series originating from the ground state $^2P^o_{3/2}$ and from the metastable $^2P^o_{1/2}$ of the Kr^+ ion. These Rydberg resonance series converge, respectively, to the $Kr^{2+}(4s^24p^4)$ $^1D_2$, $^1S_0$ thresholds, and the $Kr^{2+}(4s4p^5)$ $^3P^o_{2,1,0}$ thresholds. The energy levels tabulated

TABLE II. Principal quantum numbers n, resonance energies (eV), and quantum defects μ of the higher lying $Kr^+[4s4p^5$ ($^3P^o_2$, $^3P^o_1$)]nd series. The assignments are plotted in Fig. 1. Resonance energies are calibrated to ±30 meV and quantum defects are estimated to within an error of 20%. The spectral assignments are uncertain for entries in parentheses.

		Rydberg series $^3P^o_2$		Rydberg series $^3P^o_1$	
Initial state	n	E_n (eV)	μ	E_n (eV)	μ
$^2P^o_{3/2}$	[4d]	31.293	0.322	31.622	0.338
	5	34.863	0.320	(35.238)	(0.340)
	6	(36.335)	(0.377)	–	–
	.	.	.	.	.
	∞	38.882		39.301	

TABLE III. Principal quantum numbers n, resonance energies (eV), and quantum defects μ of the $Kr^+[4s^24p^4(^1D_2,^1S_0)]ns,nd$ series. Resonance energies are calibrated to ±30 meV and quantum defects are estimated to within an error of 20%. The assignments are plotted in Fig. 3. The spectral assignments are uncertain for entries in parentheses.

		Rydberg series $^1D_2$		Rydberg series $^1S_0$	
Initial state	n	E_n (eV)	μ	E_n (eV)	μ
$^2P^o_{3/2}$	[6s]	24.590	0.197		
	7	25.029	0.200		
	8	25.313	0.196		
	9	25.505	0.192		
	10	25.633	0.256		
	11	(25.745)	(0.141)		
	12	(25.820)	(0.124)		
	13	(25.880)	(0.090)		
	14	(25.926)	(0.066)		
	15	25.965	−0.005		
	16	25.997	−0.100		
	17	26.022	−0.011		
	18	26.043	−0.007		
	19	26.062	−0.008		
	20	26.077	−0.011		
	21	26.090	−0.012		
	.	.	.		
	∞	26.207			
$^2P^o_{3/2}$	[4d]	–	–	(24.366)	(0.373)
	5	24.342	−0.385	(25.947)	(0.385)
	6	24.878	−0.370	26.780	0.379
	7	25.217	−0.370	(27.261)	(0.379)
	8	25.441	−0.370	27.566	0.376
	9	25.598	−0.360	27.770	0.378
	10	25.712	−0.358	27.914	0.381
	11	25.796	−0.345	28.020	0.383
	12	(25.880)	(−0.671)	28.099	0.381
	13	(25.926)	(−0.633)	(28.160)	(0.394)
	14	–	–	(28.208)	(0.394)
	15	–	–	(28.247)	(0.418)
	.	.	.	.	.
	∞	26.217		28.503	

TABLE IV. Principal quantum numbers n, resonance energies (eV), and quantum defects μ of the $Kr^+[4s^24p^4(^3P_2,^3P_1)]ns$ series. Resonance energies are calibrated to ±30 meV and quantum defects are estimated to within an error of 20%. The assignments are plotted in Fig. 3. The spectral assignments are uncertain for entries in parentheses.

		Rydberg series $^3P_0$		Rydberg series $^3P_1$	
Initial state	n	E_n (eV)	μ	E_n (eV)	μ
$^2P^o_{1/2}$					
	[11s]	(23.906)	(−0.716)	–	–
	12	23.969	−0.779	–	–
	13	24.016	−0.791	–	–
	14	(24.059)	(−0.940)	–	–
	15	24.083	−0.730	23.996	0.403
	16	24.109	−0.774	–	–
	17	(24.129)	(−0.686)	–	–
	18	(24.147)	(−0.707)	–	–
	19	(24.162)	(−0.659)	–	–
	20	(24.176)	(−0.731)	–	–
	.	.	.	.	.
	∞	24.303		24.252	

TABLE V. Principal quantum numbers n, resonance energies (eV), and quantum defects μ of the $Kr^+[4s^24p^4(^1D_2,^1S_0)]ns,nd$ series. Resonance energies are calibrated to ±30 meV and quantum defects are estimated to within an error of 20%. The assignments are plotted in Fig. 3. The spectral assignments are uncertain for entries in parentheses.

		Rydberg series $^1D_2$		Rydberg series $^1S_0$	
Initial state	n	E_n (eV)	μ	E_n (eV)	μ
$^2P^o_{1/2}$					
	[6s]	23.927	0.200 ± 0.054		
	7	(24.366)	(0.205)		
	8	24.650	0.204		
	9	24.842	0.201		
	10	–	–		
	11	25.082	0.152		
	12	25.158	0.139		
	.	.	.		
	∞	25.545			
$^2P^o_{1/2}$					
	[4d]	–	–	23.738	0.358
	5	–	–	25.312	0.360
	6	24.214	−0.375	26.124	0.368
	7	24.551	−0.371	26.602	0.371
	8	24.775	−0.371	26.904	0.376
	9	24.933	−0.375	27.108	0.377
	10	25.047	−0.379	(27.261)	(0.303)
	11	25.132	−0.363	27.356	0.400
	12	25.196	−0.349	(27.435)	(0.412)
	13	25.248	−0.364	(27.495)	(0.435)
	14	–	–	(27.544)	(0.436)
	.	.	.	.	.
	∞	25.555		27.840	

from Refs. [39,40] and from the NIST tabulations [38] were used as a helpful guide for the present assignments.

The resonance series identification can be made from Rydberg's formula:

$$\epsilon_n = \epsilon_\infty - \frac{\mathcal{Z}^2}{\nu^2}, \tag{3}$$

where in Rydbergs ϵ_n is the transition energy, ϵ_∞ is the ionization potential of the excited electron to the corresponding final state ($n = \infty$), that is, the resonance series limit [41] and n being the principal quantum number. The relationship between the principal quantum number n, the effective quantum number ν, and the quantum defect μ for an ion of effective charge $\mathcal{Z}$ is given by $\nu = \mathrm{n} - \mu$. Converting all quantities to eV we can represent the Rydberg resonance series as

$$E_n = E_\infty - \frac{\mathcal{Z}^2\mathcal{R}}{(n-\mu)^2}. \tag{4}$$

Here, E_n is the resonance energy, E_∞ the resonance series limit, $\mathcal{Z}$ is the charge of the core (in this case $\mathcal{Z} = 2$), μ is the quantum defect, being zero for a pure hydrogenic state, and $\mathcal{R}$ is 13.6057 eV.

The ionization threshold from the ground state of the Kr^+ ion to that of the Kr^{2+} ion is extremely difficult to extract from the measurements due to the presence of three resonance features in that energy range: $(^1D_2)5d$, $(^1S_0)4d$ both originating from the ground state, and with $(^1D_2)7s$ originating from the metastable state.

Below the $Kr^+(^2P^o_{3/2})$ ground-state threshold, all transitions originate from the $(^2P^o_{1/2})$ metastable of Kr^+. The largest structure at 23.927 eV is assigned to the transition associated with the $(^1D_2)6s$ state. This series was assigned up to $n = 12$ (see Table V) except for the $n = 10$ peak which is not well resolved in the spectrum. The first resonance peak at 23.738 eV is attributed to the transition associated with the $(^1S_0)4d$ state: Resonance energies up to $n = 14$ for this series are listed in Table V. The transition to the $(^1S_0)10d$ resonance state interferes with that originating from the $^2P^o_{3/2}$ ground state to the $(^1S_0)7d$ level and its assignment is uncertain, for this series. We note that the intensity of the resonance structure decreases significantly above $n = 12$.

Rydberg resonance series originating from the $Kr^+(4s^24p^5\ ^2P^o_{1/2})$ metastable state converging to the $Kr^{2+}(4s^24p^4\ ^3P_0)$ threshold can be followed up to $n = 20$. The intensity of its first resonance peak ($n = 11$) is low probably due to interference with the largest resonance structure below threshold. For series converging to the $Kr^{2+}(4s^24p^4\ ^3P_1)$ threshold originating from the metastable $Kr^+(4s^24p^5\ ^2P^o_{1/2})$ state experimentally we were only able to assign one resonance feature, namely the $4s^24p^4(^3P_1)15d$ resonance state. From all our resonance analysis we estimate that our quantum defects are accurate to within 20%.

The effect of a small fraction of higher-order radiation from the undulator and dispersed by the monochromator may be more significant than was originally considered at photon energies in the 20- to 25-eV range. Recently it was realized that higher-order radiation from the undulator could be considerable [42–45]. The second peak below threshold, we tentatively speculate the assignment to be an unidentified Rydberg series converging to a limit of 25.958 eV with resolved resonance

members for $n = 5$ to 8. One possible assignment to this series is a Rydberg series originated from the $Kr^+(4s^24p^5\ ^2P^o_{3/2})$ ground state to the $Kr^+\ 4s^24p^3(^4S^o)nd(^3D^o)mg$ transitions, caused by second-order radiation in the photon beam. However, this assignment is unclear because its energy limit is shifted by 0.066 eV from the NIST tabulated value.

Above the ground-state ionization threshold, Rydberg resonance series originate from both the initial metastable $Kr^+(^2P^o_{1/2})$ and the ground state $Kr^+(^2P^o_{3/2})$ and converge, respectively, to the $Kr^{2+}(4s^24p^4\ ^1D_2,\ ^1S_0)$ thresholds. For example, in Fig. 3, two series converging to the $Kr^{2+}(4s^24p^4\ ^1S_0)$ threshold are indicated by inclined lines. The ionization potential difference of these two series is 0.663 eV which is consistent with the value of 0.666 eV tabulated by NIST [38].

The quantum defects μ of each of the Rydberg resonance series $4s^24p^4(^1S_0)nd$ converging to the $Kr^{2+}(4s^24p^4\ ^1S_0)$ threshold originating from the $^2P^o_{3/2}$ initial ground state, respectively, show a nearly constant value. Any changes we attribute to the interference with the neighboring resonance structures. They have an average value of 0.385 ± 0.08. Similarly for the quantum defects of the corresponding Rydberg resonance series $4s^24p^4(^1S_0)nd$ originating from the $^2P^o_{1/2}$ metastable state show a monotonically increasing value with an average of 0.381 ± 0.08. These compare favorably with the average value of 0.331 from the work of McLaughlin and Ballance [20]. The Rydberg resonance series $4s^24p^4(^1D_2)ns$ converging to the $(^1D_2)$ threshold have quantum defects $\mu \sim$ of 0.2 ± 0.04 or less consistent with current average estimates of 0.19. Quantum defect values (μ) for Rydberg resonance series $4s^24p^4(^1D_2)ns,md$ as measured by Ruščić *et al.* [21] for Kr^+-like atomic Bromine converging to $(^1D_2)$ threshold are consistent with the present values. For the case of the quantum defect values (μ) reported by Bizau *et al.* [3], the agreement is qualitatively consistent for states converging to the $^1S_0$ threshold.

Some of the features found in the spectrum could not be assigned, in particular, the large peak at 24.526 eV and the structures in the range 24.678–24.746 eV remain as yet unidentified.

V. DISCUSSION

The higher-resolution ALS experimental PI cross-section measurements were taken at 7.5 meV FWHM compared to the ASTRID and SOLEIL measurements obtained at the lower spectral energy resolution of 30-meV FWHM. To simulate the ALS experimental conditions the DARC theoretical PI cross sections were convoluted with a Gaussian of 7.5 meV FWHM and statistically averaged. In prior comparisons of the DARC PI cross sections with the ASTRID and SOLEIL measurements taken at a spectral resolution of 30-meV FWHM [20], the hypothesis of statistical population was justified since the lifetime is huge (0.35 s for the case of Kr^+) if compared to the beam transport times (microseconds). Excited $^2P^o_{1/2}$ metastable Kr^+ ions produced either in an ion source or ion trap rarely collide with surfaces or residual gas before photoionization takes place. Statistical population of the ions seems consistent with their measurements both accelerating ions from an ion source and using an ion trap without delay [3]. For the case of Kr^+ ions studied here we note that the theoretical results obtained from the DARC codes for the resonance positions and quantum defects are in reasonable agreement with the experimental measurements made at ASTRID and SOLEIL [3] where a statistical weighting of the initial states was assumed [20]. Taking this into account, Fig. 4 indicates for the spectral range investigated the magnitude and shape of the absolute cross sections are in excellent agreement with the previous ASTRID and SOLEIL experimental data taken at the lower resolution of 30 meV, along with the resonance energy positions. The same photon energy range is shown in Fig. 5 where the prominent Rydberg resonance series are highlighted and compared with the higher resolution ALS measurements. Here again we have excellent agreement between theory and experiment.

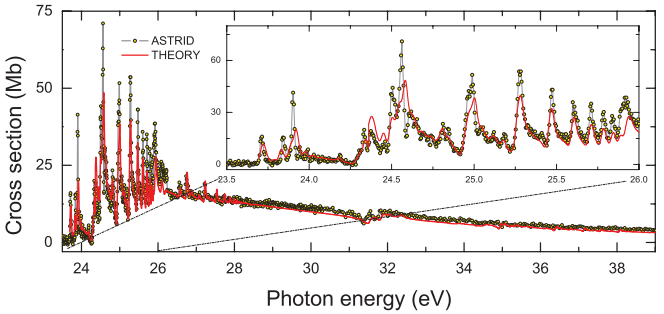

FIG. 4. (Color online) An overview of measurements for the absolute single photoionization measurements of Kr^+ ions as a function of the photon energy measured with theoretical estimates for cross sections. The ASTRID and SOLEIL measurements are at a nominal energy resolution of 30 meV. Theoretical results were obtained from a Dirac-Coulomb *R*-matrix method, convoluted with the appropriate Gaussian of full width at half maximum (FWHM) and a statistical admixture of 2/3 ground and 1/3 metastable states.

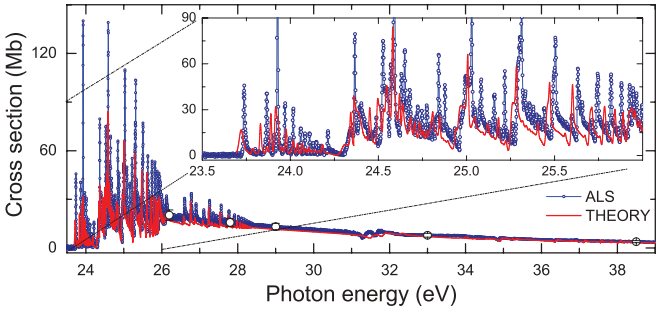

FIG. 5. (Color online) An overview of measurements for the absolute single photoionization measurements of Kr^+ ions as a function of the photon energy measured with theoretical estimates for cross sections. The ALS measurements are at a nominal energy resolution of 7.5 meV and normalized to the ASTRID and SOLEIL measurements at 26.5025 eV. Theoretical results were obtained from a Dirac-Coulomb *R*-matrix method, convoluted with the appropriate Gaussian of FWHM and a statistical admixture of 2/3 ground and 1/3 metastable states.

The integrated oscillator strengths f of the spectra, calculated using [46]

$$f = 9.11 \times 10^{-3} \int \sigma(h\nu) dh\nu, \quad (5)$$

gives a value of 1.40 ± 0.10 from the ASTRID and SOLEIL measurements of Bizau and co-workers [3]. From the DARC *R*-matrix PI cross-section calculations we obtain a value of 1.34, in excellent agreement with the previous lower resolution ASTRID and SOLEIL measurements. The present absolute measurements from the ALS yield an oscillator strength of 1.10 ± 0.25 over the same energy range. As previously noted, this difference is attributed to an overestimate of the photon flux due to a small fraction of higher-order radiation in the photon beam.

VI. SUMMARY

Photoionization cross sections were measured for a statistical admixture of ground-state and metastable Kr^+ ions in the photon energy range 23.3–39.0 eV with a spectral energy resolution of 7.5 meV. The quantum defects for each of the Rydberg series are estimated to have an uncertainty of 20% and resonance energies an uncertainty of ± 30 meV. The dominant features were spectroscopically assigned to Rydberg series and quantum defects were determined. The absolute measurements reported here are in agreement with recent measurements by Bizau *et al.* [3] within their combined systematic uncertainties. The higher energy resolution of the present measurements permitted additional resonance structures to be identified and additional spectroscopic assignments to be made. Comparisons of the statistically averaged PI cross-section calculations from the Dirac atomic *R*-matrix codes with measurements, particularly in the resonant region are in excellent agreement with the ALS higher resolution measurements and with the lower resolution measurements from ASTRID. Overall excellent agreement is seen between experiment and theory for this complicated *trans*-Fe element for the entire photon energy investigated. The present data render much higher resolution data than previous measurements [3], providing better assignments to spectroscopic features and have been benchmarked against state-of-the-art PI calculations using the Dirac atomic *R*-matrix codes. The photoionization cross sections from the present study are suitable to be included into state-of-the-art photoionization modeling codes such as CLOUDY [47,48], XSTAR [49], and ATOMDB [50] that are used to numerically simulate the thermal and ionization structure of ionized astrophysical nebulae.

ACKNOWLEDGMENTS

We thank J. M. Bizau from the Université Paris-Sud, France for the published merged-beam data from his group to compare with the present work. The experimental work was supported by the Office of Basic Energy Sciences, Chemical Sciences, Geosciences and Energy Biosciences Division, of the US Department of Energy under Grants No. DE-FG03-00ER14787 and No. DE-FG02-03ER15424 with the University of Nevada, Reno; by the Nevada DOE/EPSCoR Program in Chemical Physics, and by CONACyT, Cuernavaca, México. I.Á., C.C., and G.H. acknowledge Grants No. DGAPA UNAM-IN 113010, through ICF-UNAM, Cuernavaca, México. M.M.S'A. acknowledges support from CNPq (Brazil). C.P.B. was supported by US Department of Energy (DoE) grants through Auburn University. B.M.M. acknowledges support from the US National Science Foundation under the visitors program through a grant to ITAMP at the Harvard-Smithsonian Center for Astrophysics. The computational work was performed at the National Energy Research Scientific Computing Center in Oakland, CA, and on the Kraken XT5 facility at the National Institute for Computational Science (NICS) in Knoxville, TN. The Kraken XT5 facility is a resource of the Extreme Science and Engineering Discovery Environment (XSEDE), which is supported by National Science Foundation Grant No. OCI-1053575. The Advanced Light Source is supported by the Director, Office of Science, Office of Basic Energy Sciences, of the US Department of Energy under Contract No. DE-AC02-05CH11231.

[1] E. Cartlidge, Science **336**, 1095 (2012).
[2] N. C. Sterling, H. L. Dinerstein, and T. R. Kallman, Astrophys. J. Suppl. Ser. **169**, 37 (2007).
[3] J. M. Bizau, C. Blancard, M. Coreno, D. Cubaynes, C. Dehon, N. E. Hassan, F. Folkmann, M. F. Gharaibeh, A. Giuliani, J. Lemaire, A. R. Milosavljevi, C. Nicolas, and R. Thissen, J. Phys. B **44**, 055205 (2011).
[4] M. Bakhtiari, H. Tamai, Y. Kawano, G. Kramer, A. Isayama, T. Nakano, Y. Kamiya, R. Yoshino, Y. Miura, Y. Kusama, and Y. Nishida, Nucl. Fusion **45**, 318 (2005).
[5] N. C. Sterling, Astron. Astrophys. **533**, A62 (2011).
[6] B. Sharpee, Y. Zhang, R. Williams, E. Pellegrini, K. Cavagnolo, J. A. Badwin, M. Phillips, and X. W. Lui, Astrophys. J. **659**, 1265 (2007).
[7] C. Sneden, J. Cowan, and R. Gallino, Annu. Rev. Astron. Astrophys **46**, 241 (2008).
[8] M. Lu, G. Alna'washi, M. Habibi, M. F. Gharaibeh, R. A. Phaneuf, A. L. D. Kilcoyne, E. Levenson, A. S. Schlachter, C. Cisneros, and G. Hinojosa, Phys. Rev. A **74**, 062701 (2006).
[9] M. Lu, M. F. Gharaibeh, G. Alna'washi, R. A. Phaneuf, A. L. D. Kilcoyne, E. Levenson, A. S. Schlachter, A. Müller, S. Schippers, J. Jacobi, S. W. J. Scully, and C. Cisneros, Phys. Rev. A **74**, 012703 (2006).
[10] D. Kilbane, F. Folkmann, J. M. Bizau, C. Banahan, S. W. J. Scully, H. Kjeldsen, P. van Kampen, M. W. D. Mansfield, J. T. Costello, and J. B. West, Phys. Rev. A **75**, 032711 (2007).
[11] S. H. Southworth, D. A. Arms, E. M. Dufresne, R. W. Dunford, D. L. Ederer, C. Höhr, E. P. Kanter, B. Krässig, E. C. Landahl, E. R. Peterson, J. Rudati, R. Santra, D. A. Walko, and L. Young, Phys. Rev. A **76**, 043421 (2007).
[12] M. Richter, M. Y. Amusia, S. V. Bobashev, T. Feigl, P. N. Juranić, M. Martins, A. A. Sorokin, and K. Tiedtke, Phys. Rev. Lett. **102**, 163002 (2009).

[13] M. Meyer, D. Cubaynes, V. Richardson, J. T. Costello, P. Radcliffe, W. B. Li, S. Düsterer, S. Fritzsche, A. Mihelic, K. G. Papamihail, and P. Lambropoulos, Phys. Rev. Lett. **104**, 213001 (2010).
[14] J. B. West, J. Phys. B **34**, R45 (2001).
[15] H. Kjeldsen, J. Phys. B **39**, R325 (2006).
[16] P. G. Burke and W. D. Robb, *Advances in Atomic and Molecular Physics*, Vol. 11 (Academic Press, New York, 1975).
[17] P. G. Burke, *R-Matrix Theory of Atomic Collisions: Application to Atomic, Molecular and Optical Processes* (Springer, New York, 2011).
[18] A. M. Covington, A. Aguilar, I. R. Covington, G. Hinojosa, C. A. Shirley, R. A. Phaneuf, I. Álvarez, C. Cisneros, I. Dominguez-Lopez, M. M. Sant'Anna, A. S. Schlachter, C. P. Ballance, and B. M. McLaughlin, Phys. Rev. A **84**, 013413 (2011).
[19] N. C. Sterling and H. L. Dinerstein, Astrophys. J. Suppl. Ser. **174**, 158 (2008).
[20] B. M. McLaughlin and C. P. Ballance, J. Phys. B **45**, 085701 (2012).
[21] B. Ruscic, J. P. Greene, and J. Berkowitz, J. Phys. B **17**, 1503 (1984).
[22] P. van der Meulen, M. O. Krause, and C. A. deLange, J. Phys. B **25**, 97 (1992).
[23] R. A. Phaneuf, C. C. Havener, G. H. Dunn, and A. Müller, Rep. Prog. Phys. **62**, 1143 (1999).
[24] A. M. Covington, A. Aguilar, I. R. Covington, M. F. Gharaibeh, G. Hinojosa, C. A. Shirley, R. A. Phaneuf, I. Álvarez, C. Cisneros, I. Dominguez-Lopez, M. M. Sant'Anna, A. S. Schlachter, B. M. McLaughlin, and A. Dalgarno, Phys. Rev. A **66**, 062710 (2002).
[25] G. Hinojosa, A. M. Covington, R. A. Phaneuf, M. M. Sant'Anna, R. Hernandez, I. R. Covington, I. Dominguez, J. D. Bozek, A. S. Schlachter, I. Álvarez, and C. Cisneros, Phys. Rev. A **66**, 032718 (2002).
[26] A. M. Covington, A. Aguilar, I. R. Covington, M. Gharaibeh, C. A. Shirley, R. A. Phaneuf, I. Álvarez, C. Cisneros, G. Hinojosa, J. D. Bozek, I. Dominguez, M. M. Sant'Anna, A. S. Schlachter, N. Berrah, S. N. Nahar, and B. M. McLaughlin, Phys. Rev. Lett. **87**, 243002 (2001).
[27] A. Aguilar, A. M. Covington, G. Hinojosa, R. A. Phaneuf, I. Álvarez, C. Cisneros, J. D. Bozek, I. Dominguez, M. M. Sant'Anna, A. S. Schlachter, S. N. Nahar, and B. M. McLaughlin, Astrophys. J. Suppl. Ser. **146**, 467 (2003).
[28] N. G. Adams, D. Smith, and E. Alge, J. Phys. B **13**, 3235 (1980).
[29] A. Kok, P. A. Z. van Emmichoven, and A. Niehaus, Chem. Phys. **258**, 47 (2000).
[30] C. P. Ballance and D. C. Griffin, J. Phys. B **39**, 3617 (2006).
[31] P. H. Norrington and I. P. Grant, J. Phys. B **20**, 4869 (1987).
[32] W. P. Wijesundera, F. A. Parpia, I. P. Grant, and P. H. Norrington, J. Phys. B **24**, 1803 (1991).
[33] P. H. Norrington, J. Phys. B **24**, 1803 (1991).
[34] P. H. Norrington, DARC codes [http://web.am.qub.ac.uk/DARC].
[35] V. Fivet, M. A. Bautista, and C. P. Ballance, J. Phys. B **45**, 035201 (2012).
[36] B. M. McLaughlin and C. P. Ballance, J. Phys. B **45**, 095202 (2012).
[37] A. Müller, S. Schippers, J. Hellhund, A. L. D. Kilcoyne, R. A. Phaneuf, C. P. Ballance, and B. M. McLaughlin (unpublished).
[38] Y. Ralchenko, A. E. Kramida, J. Reader, and N. A. T. *NIST Atomic Spectra Database*, Version 4.0.1 (National Institute of Standards and Technology, Gaithersburg, 2011).
[39] J. Sugar and A. Musgrove, J. Phys. Chem. Ref. Data **20**, 859 (1991).
[40] E. B. Saloman, J. Phys. Chem. Ref. Data **36**, 215 (2007).
[41] M. J. Seaton, Rep. Prog. Phys. **46**, 167 (1983).
[42] D. A. Esteves, Ph.D. thesis, University of Reno, 2010.
[43] D. A. Esteves, R. C. Bilodeau, N. C. Sterling, R. A. Phaneuf, A. L. D. Kilcoyne, E. C. Red, and A. Aguilar, Phys. Rev. A **84**, 013406 (2011).
[44] N. C. Sterling, D. A. Esteves, R. C. Bilodeau, A. L. D. Kilcoyne, E. C. Red, R. A. Phaneuf, and A. Aguilar, J. Phys. B **44**, 025701 (2011).
[45] N. C. Sterling, M. C. Witthoeft, D. A. Esteves, R. C. Bilodeau, A. L. D. Kilcoyne, E. C. Red, R. A. Phaneuf, G. AlnaWashi, and A. Aguilar, Can. J. Phys. **89**, 379 (2011).
[46] U. Fano, and J. W. Cooper, Rev. Mod. Phys. **40**, 441 (1968).
[47] G. Ferland, K. T. Korista, D. A. Verner, J. W. Ferguson, J. B. Kingdon, and E. M. Verner, Pub. Astron. Soc. Pac. (*PASP*) **110**, 761 (1998).
[48] G. J. Ferland, Annu. Rev. Astron. Astrophys. **41**, 517 (2003).
[49] T. R. Kallman, Astrophys. J. Suppl. Ser. **134**, 139 (2001).
[50] A. R. Foster, L. Ji, R. K. Smith, and N. S. Brickhouse, Astrophys. J. **756**, 128 (2012).